

# A density-functional study of charge doping in $\text{W O}_3$

Andrew D. Walkingshaw, Nicola A. Spaldin, and Emilio Artacho

Department of Earth Sciences, University of Cambridge, Downing Street, Cambridge CB2 3EQ, UK

(Dated: March 22, 2024)

The addition of electron donors to the vacant A site of defect-perovskite structure tungsten trioxide causes a series of structural and chemical phase transitions; for instance, in the well-known case of the sodium tungsten bronzes ( $\text{Na}_x\text{W O}_3$ ). Here we calculate the effect of the addition of electronic charge to  $\text{W O}_3$  without the complication of also including sodium ions. Our density functional theory method enables isolation of electronic effects from the additional size, chemical, and disorder effects present in experimental samples. Our calculated low-temperature phase diagram between  $x=0$  and  $x=1$  moves from the initial low-temperature monoclinic phase through a second (centered) monoclinic phase, an orthorhombic phase, a tetragonal antiferroelectric, and an aristotypic cubic phase, in broad agreement with the experimentally-observed transformations in  $\text{Na}_x\text{W O}_3$ . Our work confirms that the observed structural transformations are driven primarily by electronic factors. We find that the dominant electronic effect is the covalent interaction between the tungsten 5d and oxygen 2p orbitals.

PACS numbers: 61.72.Ww, 71.15.Mb, 71.20.Nr, 71.30.Bh, 71.38.Ht

## I. INTRODUCTION

Tungsten trioxide,  $\text{W O}_3$ , is a technologically-significant ceramic: it is electrochromic<sup>1</sup>, and the possibility of ion intercalation and deintercalation gives rise to several potential applications in devices (for instance, as a cathode of rechargeable batteries<sup>2</sup>). In particular, it is often used in optical applications due to the fact that the color can be changed by doping with electrons. (This was first observed in 1815 by Berzelius<sup>3</sup> in  $\text{H}_x\text{W O}_3$ ). Bulk stoichiometric  $\text{W O}_3$  is yellow-green in hue, but the sodium-doped tungsten bronzes,  $\text{Na}_x\text{W O}_3$ , exhibit most colors of the visible spectrum on varying Na concentration<sup>4</sup>. In addition, the optical absorbance and reactivity of the material can be modulated by injection or extraction of electrons and ions, giving excellent control over and tunability to the optical properties<sup>1,5</sup>.

In addition to strongly affecting the color of the material, the incorporation of electron donating ions also has a strong effect on the structure. For example, complex structural behaviour is observed on doping with electron donors, such as Na, Li or H. Such dopants occupy the vacant perovskite A site and therefore they can be easily introduced over a wide range of concentrations, from trace concentrations in the so-called phase up to the limiting case of the tungsten bronze,  $\text{NaW O}_3$ . In  $\text{NaW O}_3$ , there is one donor per formula unit, and an aristotypic perovskite structure is adopted<sup>6</sup>. Its structure is the same as that of  $\text{ReO}_3$ , with both solids retaining the ideal cubic perovskite structure at all temperatures. Indeed, assuming that in  $\text{NaW O}_3$  the valence electron of Na is donated into the 5d-type conduction/antibonding band of  $\text{W O}_3$ , the two materials are isoelectronic. In contrast,  $\text{W O}_3$  displays both off-centering of the W ion from its ideal centrosymmetric position, and Glazer<sup>7</sup>-type tilting transitions. Studies on intermediate concentrations of  $\text{Na}_x\text{W O}_3$ <sup>8</sup> suggest a complex phenomenology, involving a consistent reduction in the degree of polyhe-

dral tilting with increasing dopant concentration. Notably, Clarke observed that the room-temperature structures of  $\text{Na}_x\text{W O}_3$  ( $0.62 < x < 0.94$ ) are slightly distorted from the high-symmetry  $\text{Pm}3\text{m}$  aristotype, and proposed a preliminary phase diagram to explain the observed diffraction data<sup>8</sup>.

There have been several prior computational studies on  $\text{W O}_3$ , carried out at various levels of theory. Here we summarize the results of the density functional theory (DFT) studies from the literature. Perhaps the most relevant for our study is the work by Cora et al.<sup>9,10</sup> on the electronic structure of cubic  $\text{W O}_3$ ,  $\text{ReO}_3$  and  $\text{NaW O}_3$ . Using the full potential linear muffin-tin orbital method, with the local density approximation, they showed that the band structures of the three compounds are very similar, with the extra electron in  $\text{ReO}_3$  and  $\text{NaW O}_3$  occupying the antibonding conduction band and decreasing the metal-oxygen bonding strength. They also showed that displacement of the transition metal from its centrosymmetric position towards an oxygen ion causes increased hybridization of the transition metal 5d  $t_{2g}$  orbitals at the bottom of the conduction band with the O 2p orbitals at the top of the valence band. This in turn lowers the energy of the top of the valence band, and raises that of the bottom of the conduction band, explaining why metallic  $\text{ReO}_3$  and  $\text{NaW O}_3$  remain cubic, whereas  $\text{d}^0$   $\text{W O}_3$ <sup>11</sup> has an off-centering distortion. Hjelm et al.<sup>12</sup> used the same method to establish that, in  $\text{LiW O}_3$  and  $\text{NaW O}_3$ , rigid band filling of the  $\text{W O}_3$  conduction band occurs, whereas in  $\text{HW O}_3$  the hydrogens form hydroxide units with the oxygen atoms and change the electronic structure. de Wijs et al.<sup>13</sup> calculated the electronic properties of the various experimental structural phases of  $\text{W O}_3$  using a plane wave ultra-soft pseudopotential implementation of DFT within both the generalized gradient and local density approximations. They found that increases in pressure are readily accommodated by tilting of the octahedra, explaining the small experimental bulk

Species	n	l	$r(1)$	$r(2)$
W	6	0	6.50	5.00
	5	2	6.49	3.75
	6	1	6.49	n/a
O	2	0	3.31	2.51
	2	1	3.94	2.58
	3	2	3.94	n/a

TABLE I: Cutoff radii,  $r()$ , for the basis sets corresponding to W and O species; as the basis set is double- $\zeta$  polarized, there are two basis functions (and therefore radii) per hypothetical atomic orbital, as specified by quantum numbers  $n$  and  $l$ . All radii are given in bohr. The starred entries are polarization orbitals.

modulus. Also, they observed large W displacements, accompanied by strong rehybridization and changes in the electronic band gaps. This latter observation is consistent with the anomalously large Born effective charges calculated for cubic  $\text{WO}_3$  by Detraux et al.<sup>14</sup>.

The work presented here builds on these earlier theoretical studies by treating fractional doping effects (i.e., the effect of electron concentrations between 0 and 1 per W ion) in a fully self-consistent manner. Our computational approach allows the isolation of the effects of additional valence electrons from other factors, such as the presence of donor cations and structural disorder at intermediate concentrations. Indeed, it has already been shown that simple model calculations including only electronic effects can reproduce some aspects of the observed structural behavior<sup>9</sup>. Our main result is that electronic effects are able to account fully for the experimentally observed structural phase transitions.

## II. METHODOLOGY

Calculations were performed using the Siesta implementation<sup>15,16</sup>, of density-functional theory<sup>17</sup> (DFT), within the Perdew-Zunger<sup>18</sup> parametrization of the local-density approximation<sup>19</sup>. Core electrons were replaced by norm-conserving Trouiller-Martins<sup>20</sup> pseudopotentials, factorised as prescribed by Kleinman and Bylander.<sup>21</sup> The valence electrons were taken to be  $2s^2 2p^4$  for O, and  $6s^2 5d^4$  for W. Wave-functions were expanded in a basis of numerical atomic orbitals of finite support<sup>22</sup>. A double- $\zeta$  polarised (DZP) basis set was used, whereby two basis functions per valence atomic orbital are included, plus extra shells of higher angular momentum to allow polarization. This size of basis has been found, in prior studies, to give results of similar quality to typical plane-wave basis sets in other major codes. Details for the pseudopotentials and the basis sets are given in Tables I and II.

For  $k$ -point sampling, a cutoff of 10 Å was used<sup>24</sup>; this gave 24 independent  $k$ -points in the first Brillouin zone

Species	s	p	d	f
W ( $5d^4 6s^2$ )	2.85	3.03	2.25	2.25
O ( $2s^2 2p^4$ )	1.15	1.15	1.15	1.15

TABLE II: Concomitant radii for each of the  $s$ ,  $p$ ,  $d$ , and  $f$  channels of our W and O pseudopotentials. All radii are given in bohr. The W pseudopotential used also included a partial-core correction, with a radius of 1.30 bohr, according to the scheme of Louie et al.<sup>23</sup>.

of the low-temperature monoclinic phase, corresponding to a  $4 \times 3 \times 3$  mesh. This is equivalent to 6 independent  $k$ -points within the first Brillouin zone of a 64-atom supercell of the same structure, corresponding to a  $2 \times 2 \times 3$  mesh (if one were to neglect degeneracy). Both  $k$ -point meshes were generated by the method of Monkhorst and Pack<sup>25</sup>. The fineness of the real-space grid used for numeric integration was set to correspond to an energy cutoff of 200 Ry. A grid-cell sampling<sup>16</sup> of four points (arranged on a face-centered cubic lattice) was used to reduce the space inhomogeneity introduced by the finite grid. All calculations were performed using variable-cell relaxation, with the convergence criteria set to correspond to a maximum residual stress of 0.01 GPa, and maximum residual force component of 0.04 eV/Å.

In order to test the quality of the pseudopotential and basis set used, we first performed calculations on the same phases as investigated by de Wijs et al. Results of comparable quality to theirs were obtained (see table III), although our results tend to give the expected underestimation of the experimental lattice parameters whereas theirs, even in the LDA, tend to overestimate.

In order to investigate the effect of additional dopant charge on the bonding character and structure of  $\text{WO}_3$ , a  $2 \times 2 \times 1$  supercell of the low-temperature monoclinic ( $P2_1$ ) phase was used (the aforementioned 64-atom supercell). This contains sixteen W centers, and can be considered to be a  $2 \times 2 \times 2 \times 2 \times 2$  supercell of the archetypic perovskite structure. As such, it is sufficiently large to encompass all ground-state symmetries experimentally observed in pure  $\text{WO}_3$ . A additional charge was added by the injection of extra electrons into the system, with charge neutrality over space being ensured by a corresponding homogeneous positively-charged background.

## III. CALCULATED PHASE DIAGRAM

We performed calculations for numbers of dopant electrons between 1 and 16 per supercell, (corresponding to electron concentrations in the range  $0 < x < 1$  per W center) in single-electron steps. Full, variable-cell, structural relaxations were performed for each doping level. A series of five phases was observed over the doping range. Here we describe the five structures in turn, starting with the highest doping level. We refer to figure 1, which

TABLE III: Lattice parameters, experimental, from our simulations, and from the work of de Wijs<sup>13</sup> for (hypothetical) cubic, low temperature monoclinic, room temperature monoclinic, high-temperature tetragonal and room temperature triclinic phases of  $\text{WO}_3$ . All distances are given in Å. Note that de Wijs' calculations were performed under the local-density approximation for monoclinic phases, and under the generalized gradient approximation for triclinic and tetragonal phases.

Phase		a	b	c			
Cubic							
	This work	3.81	3.81	3.81	90.0	90.0	90.0
Monoclinic LT							
	This work	5.15	5.05	7.63	90.0	92.6	90.0
	de Wijs	5.34	5.31	7.77	90.0	90.6	90.0
	Experiment <sup>26</sup>	5.28	5.15	7.66	90.0	91.8	90.0
Monoclinic RT							
	This work	7.30	7.49	7.32	89.8	90.1	90.0
	de Wijs	7.37	7.46	7.64	90.0	90.6	90.0
	Experiment <sup>27</sup>	7.31	7.54	7.66	90.0	91.8	90.0
Tetragonal							
	This work	5.31	5.31	3.91	90.0	90.0	90.0
	de Wijs	5.36	5.36	3.98	90.0	90.0	90.0
	Experiment <sup>28</sup>	5.27	5.27	3.92	90.0	90.0	90.0
Triclinic							
	RT						
	This work	7.18	7.36	7.63	88.0	90.5	90.4
	de Wijs	7.54	7.64	7.84	89.7	90.2	90.2
	Experiment <sup>29</sup>	7.30	7.52	7.69	88.8	90.9	91.0

shows (a) our calculated lattice parameters ( $c'$  is the  $c$  lattice parameter multiplied by  $\sqrt{2}$  in order to normalize it with respect to the  $a$  and  $b$  parameters), (b) our calculated unit cell volumes, and (c) our  $\text{W-O}$  bond lengths. Our suggested phase boundaries are also shown in figure 1 (a) as solid vertical lines.

At maximal doping, we obtain the perovskite aristotypic (i.e. the highest symmetry phase in the series: in the case of perovskites, primitive cubic,  $a = b = c$ , one formula unit per unit cell) structure, with space group  $Pm\bar{3}m$ . The three lattice parameters are equal, as are the  $\text{W-O}$  bond lengths.

With decreasing dopant concentration the unit cell volume decreases slightly, until at  $x = \frac{11}{16}$ , we find a symmetry-breaking transition to an antiferroelectric tetragonal phase with  $P4/nmm$  symmetry. The  $\text{W}$  atom moves off the center of its  $\text{O}_6$  octahedron in the  $[001]$  direction [as shown in figure 2 (a)], resulting in different  $\text{W-O}$  bond lengths and a lowering of the space group of the system. Interestingly, all three lattice parameters continue to have the same effective length with respect to our supercell (within the accuracy of our computations) in spite of the inequivalence of one of them due to the reduction in symmetry. This can be ascribed to the fact that the oxygen framework distorts very little in these

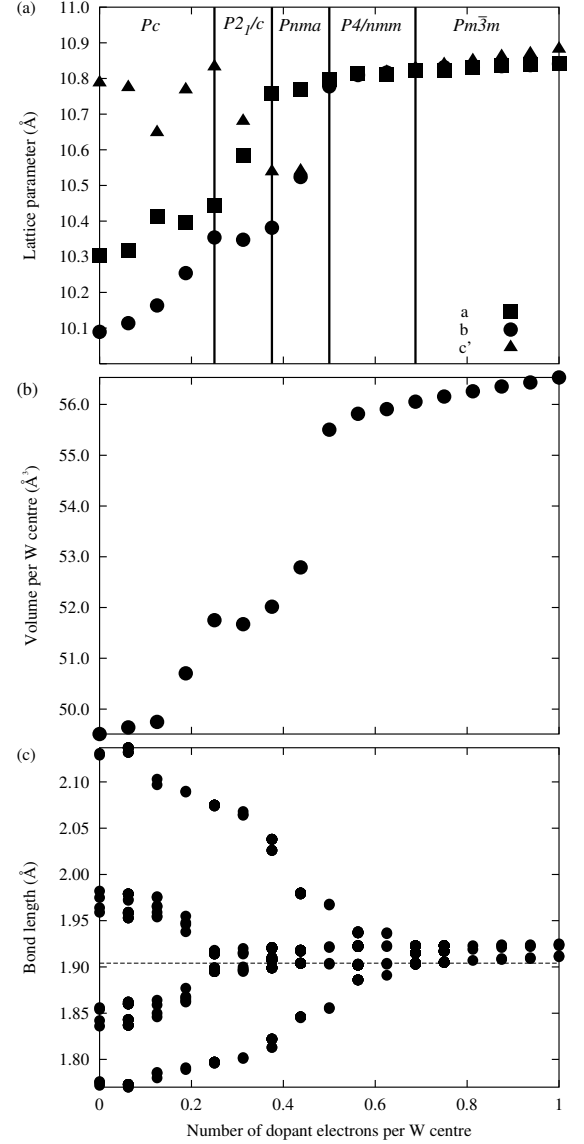


FIG. 1: (a) Lattice parameters (for normalized cubic supercell with respect to the phase) of  $\text{WO}_3$ ; (b) Volumes of  $2 \times 2 \times 2$  supercell of  $\text{WO}_3$ ; (c) Bond lengths within  $\text{WO}_6$  octahedra, all versus electron dopant concentration.

transitions, and it is the oxygen framework that is largely responsible for the volume and shape of the unit cell. The antiferroelectric tetragonal phase persists down to a dopant concentration of approximately  $\frac{1}{2}$  electron per  $\text{W}$ , with a gradual increase in  $\text{O}$ -centering with decreasing dopant concentration. By  $x = \frac{1}{2}$ , the  $\text{O}$ -centering of the  $\text{W}$  along the  $[001]$  direction has increased to around 0.08 Å.

The antiferroelectric tetragonal phase becomes unstable under  $\frac{1}{2}$  electrons per  $\text{W}$ , and an orthorhombic phase is stabilised. There is also a clear discontinuity in the volume per unit cell at this doping concentration. This arises from a tilt of the  $\text{WO}_6$  octahedra towards  $[110]$ -type directions which in turn causes the loss of the

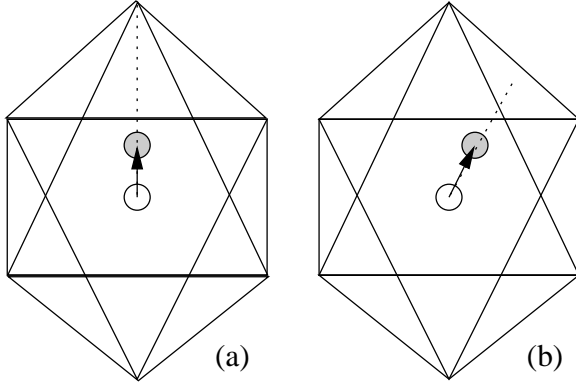


FIG. 2: O centering in  $WO_6$  octahedra; (a) along  $[001]$ , (b) along both  $[001]$  and  $[110]$ -type directions

four-fold rotation in the  $c$  direction, lowering the space group to  $Pnm\bar{a}$ . Initially, the  $c^0$  and  $a$  lattice parameters (within our pseudocubic supercell), despite being symmetrically inequivalent, remain essentially equal in length; this can be ascribed to the absence of distortion of the  $WO_6$  octahedra, which originally tilt (around an axis parallel to  $b$ ) as a rigid unit without substantial deformation. These parameters become unequal at  $x = \frac{7}{16}$ ; however, we do not find a lowering of the space group caused by this.

Below  $x = \frac{3}{8}$ , a monoclinic  $P2_1/c$  phase (similar to that identified by de Wijs<sup>13</sup>), related to the low-temperature phase in  $WO_3$ , is stable. The phase boundary from the orthorhombic to monoclinic phase is characterized by an increase in the  $W-O$  displacement along  $[001]$  (seen in the increased bond splitting in figure 1 (c)) as well as a marked rotation around  $z$  (loosely speaking in the  $xy$  plane). The Glazer tilt is expressible as  $a \neq b \neq c$ . The monoclinic symmetry persists through the remainder of the phase diagram; however an additional phase boundary exists at  $x = \frac{1}{4}$ . Here an additional splitting in the  $W-O$  bond lengths indicates off-centering of the  $W$  atom in a  $[110]$ -type direction (as shown in figure 2 (b)) and there is also a second discontinuity in the cell volume. This corresponds to a loss of screw axes along  $b$ , and hence a further lowering of the space group to  $Pc$ , the  $\beta$  phase.

Order parameters can be defined for the transitions between each of these phases as shown in figure 3. The order parameter for the  $Pc$  to  $P2_1/c$  transition (figure 3 (a)) is the difference between the  $W-O$  bond lengths in the  $xy$  plane ( $xy_1$  and  $xy_2$ ). The order parameter for the  $P2_1/c$  to  $Pnm\bar{a}$  transition is, as expected, the deviation of the angle from  $90^\circ$ ; this goes sharply to zero at  $x = \frac{3}{8}$  (figure 3 (b)). The order parameter for the  $Pnm\bar{a}$  to  $P4/nmm$  phase is the length difference between the two remaining unequal lattice constants,  $b - a$  (figure 3 (c)). Finally, the ideal cubic  $Pm\bar{3}m$  perovskite structure is reached when the  $W$  moves to its centrosymmetric position, and the order parameter for the tetragonal to the cubic phase is the magnitude of the  $W-O$ -center displacement

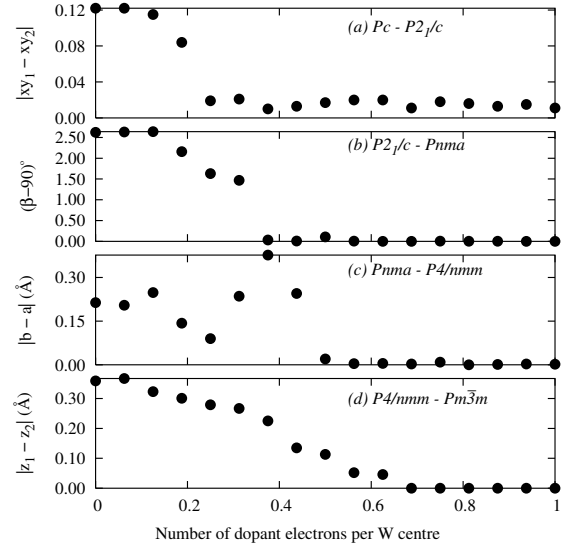


FIG. 3: Order parameters for the doping-induced phase transitions in  $WO_3$ . (a)  $Pc \{ P2_1/c$ , in Å, where  $xy_1$  and  $xy_2$  are the inequivalent  $W-O$  bond lengths in the  $xy$  plane; (b)  $P2_1/c \{ Pnm\bar{a}$ , in degrees; (c)  $Pnm\bar{a} \{ P4/nmm$  (in Å); (d)  $P4/nmm \{ Pm\bar{3}m$  (in Å), where  $z_1$  and  $z_2$  refer to the two  $W-O$  bonds aligned predominantly with the  $z$  axis.

ment along  $[001]$  (figure 3 (d)). As such, all the phase boundaries are well-defined, although further work could be undertaken to locate them with greater precision. In the next Section we discuss the effects giving rise to this phase structure in greater depth.

#### IV. DISCUSSION

We see that there are two types of structural distortion occurring in  $WO_3$ ; rotation of the (almost rigid) octahedra, and displacement of the  $W$  ion from the center of its octahedron. The occurrence or absence of  $W$  off-centering is known to be determined by a balance between electronic Coulomb repulsions (which are minimized for the centrosymmetric structure) and additional bonding considerations which might stabilize the non-centrosymmetric phase<sup>11</sup>. In the case of  $WO_3$ , off-centering of the  $W$  ion results in additional hybridizations that lower the energy of the  $O$   $2p$ -like valence band compared with that of the centered structure, and raise the energy of the predominantly  $W$   $5d$   $t_{2g}$  conduction band<sup>9</sup>. As the doping level is increased, and more electron density is added to the conduction band, there is no energetic advantage to these additional hybridizations, and the  $W$  ion moves back to its centrosymmetric position.

The fact that the small off-centering in the  $[110]$  direction is quenched first implies that the antibonding orbitals corresponding to this covalent interaction are low-lying in the conduction band and therefore filled first.

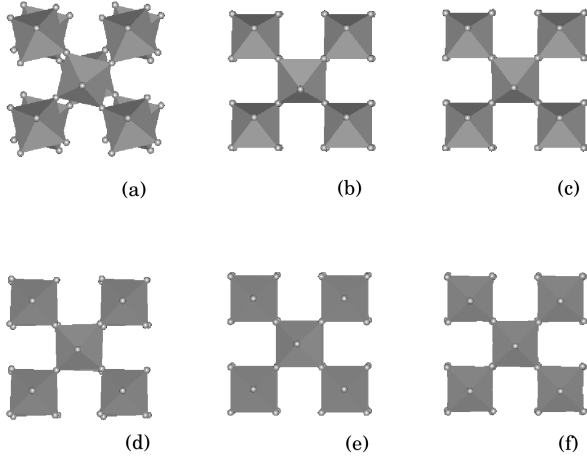


FIG. 4: Polyhedral tilts in  $\text{WO}_3$ , as varying with dopant charge. The charges in each case are, in electrons per W atom, are; (a)  $3/16$ , (b)  $5/16$ , (c)  $7/16$ , (d)  $1/2$ , (e)  $5/8$ , (f)  $1$ ; these correspond to, respectively, the monoclinic  $Pc$  phase; the  $P2_1=c$  phase, approaching the  $Pnm$  boundary; the middle of the orthorhombic phase; the  $P4=nm$  boundary; within the stability range of the tetragonal phase; and the aristotype. It is clear that the distortions between some phases are extremely small. This poses difficulties in ascertaining exactly where they are located in composition space.

The  $o$ -centering in the  $z$  direction persists to higher doping concentrations and is only quenched out at  $\frac{3}{4}$  e per center. This 75% concentration is clearly less than the value of  $0.98$  e suggested by Cora et al.'s analysis of one-electron energies for the displacement of Re along  $[100]$  in  $\text{ReO}_3$ <sup>9</sup>; this accords with their suggestion, however, that crystal field effects would favour cubic structures, and thus any analysis under a rigid-band approximation (or similar) would overestimate the degree of doping necessary to cause the onset of cubicity.

There is strong evidence of a relationship between the polyhedral rotation and  $o$ -centering mechanisms. In figure 4 we show sketches of the structures at different doping concentrations to illustrate the polyhedral tilting. At  $\frac{3}{16}$  doping (figure 4 (a)) we see that the rotations are large around both axes. However in figure 4 (b) (by which the  $o$ -centering in the  $[110]$  direction has been essentially quenched ( $\times \frac{5}{16}$ )) we see that the rotation of polyhedra in that plane also disappears, whilst rotation of polyhedra between connections along the  $z$  axis persists, as does the  $o$ -centering in that direction. This persists, with reducing magnitude, to  $\times \frac{7}{16}$  (figure 4 (c)), but by 50% doping, (figure 4 (d)) any remaining tilt up the  $z$  axis (out of the page) is extremely small. However, at this concentration,  $o$ -centering along  $[001]$  persists. Notice also that the majority of volume change in the unit cell, which in perovskites is caused by changing of the rotation angles, has also occurred by this doping level. Finally, any tilt systems in figures 4 (e) and (f), corre-

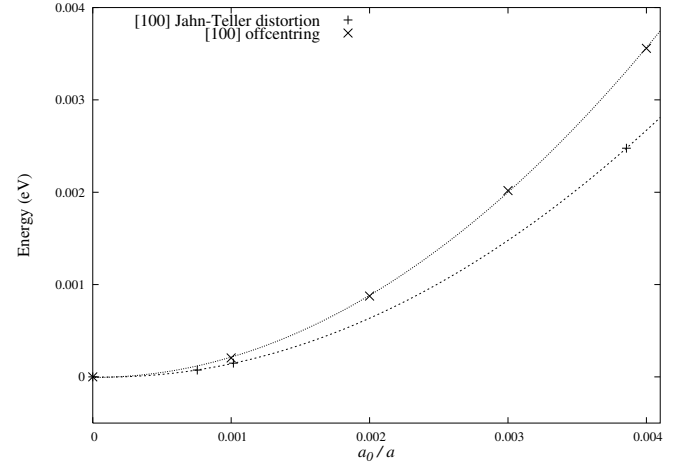


FIG. 5: Increase in energy as a function of fractional change in  $W-O$  bondlength for both  $W-O$ -centering and Jahn-Teller distortion along a cubic axis.

sponding to concentrations with centered  $W$  ions, are too small to observe in the figure.

It should be noted that the very small  $[100]$ - $o$ -centering – less than  $0.01\text{\AA}$  in magnitude – which persists at high doping concentration does not appear to be a real effect. In fact, both this and the small Jahn-Teller distortion at 100% doping appear to be numerical artifacts related to the real-space mesh cutoff used: when the mesh is increased to 500 Ry (from 200 Ry), both effects disappear. As it is computationally expensive, one cannot justify this level of convergence for all calculations, particularly given that the order parameters delineating the phase boundaries in the system are well-defined at the present level of accuracy. Even so, it is clear that the system is very near the limits where Jahn-Teller distortion and/or  $o$ -centering of the  $W$  atom become thermodynamically stable. As expected by analogy with  $\text{ReO}_3$ ,  $\text{WO}_3$  doped with 1 electron is entirely cubic, with no Jahn-Teller distortion or  $W-O$ -centering. Since the transition metal, in both cases, has a formal  $d^1$  electron configuration (and  $d^1$  ions in octahedrally coordinated complexes do not have a second-order Jahn-Teller distortion) the centrosymmetry is easy to explain. The lack of a true Jahn-Teller distortion (which is predicted for such a  $d^1$  ion in octahedral coordination) is more subtle however, and is determined by a competition between energy lowering through hybridization (strongest in the cubic structure) and energy lowering through gap formation during the distortion. In bulk  $\text{ReO}_3$ , the broad bands and low density of states at the Fermi energy result in the cubic phase having the lowest energy. In contrast, in a molecular complex the bands are infinitely narrow and the Fermi energy density of states is infinitely large (favouring Jahn-Teller distortion).

In figure 5 we plot our calculated change in energy, as a function of the amount of both Jahn-Teller distortion and transition metal  $o$ -centering, for  $\text{WO}_3$  doped

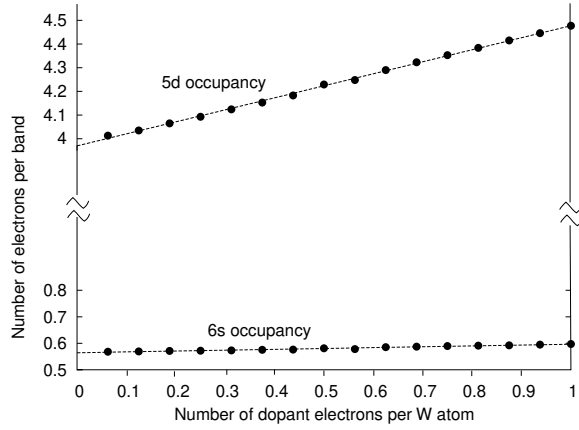


FIG. 6: Mean occupancy per W atom of 5d and 6s orbitals versus dopant charge.

with one electron per W center. In both cases a constant volume is maintained. The x axis shows the fractional change in bond length; for the Jahn-Teller distorted structure both W-O bond lengths increase by this amount, and for the o-centered structure one increases and the other decreases. Note that, by this measure, the structure is stiffer to Jahn-Teller distortion than it is to o-centering. Also note that our curvature for o-centering is very close to that of Cora et al.'s<sup>9</sup> for  $\text{ReO}_3$  (which in turn is around half that for  $\text{NaWO}_3$ ).

A Mulliken analysis of the occupancy of the three families of bands due to W { 6s,  $5d_{e_g}$ , and  $5d_{t_2g}$  } suggests that the occupancy of the 5d band is far from  $d^0$  in undoped  $\text{WO}_3$ , and far from  $d^1$  in the fully doped system. The occupancy of the d-band is closer to four in undoped  $\{\text{WO}_3\}$  (see figure 6) and increases by approximately 0.5 e in the fully doped system. The remaining half of an electron, unsurprisingly, fills the antibonding bands formed by O (2p) {W (5d) overlap. Note that the mean occupancy of the 6s orbital, which is 0.58 electrons per orbital in the undoped system, hardly increases on addition of electrons. This implies a typical W valence population of between 4.5 and 5 electrons, in contrast to the idealised purely-ionic picture of a bare  $\text{W}^{6+}$  ion (with no valence electrons); this is yet further evidence of a system remarkably dominated by covalent W-O interactions. It is clear from further analysis that above 50% doping, dopant charge preferentially fills the  $5d_{xz}$  and  $5d_{yz}$  bands; the other bands experience only a small change in total occupancy. This accords well with the suggestion that bonding (antibonding splitting occurs through O (2p)-W (5d) -like overlap; the absence of change in xy bonding being demonstrated by the absence in change of occupancy of the  $5d_{xy}$  band. However, given the tilting transitions and highly-deformed structures, there is great difficulty in assigning the occupancy of 5d orbitals; therefore, further studies of the influence of band formation and orbital occupation on both first- and second-order Jahn-Teller distortions are ongoing.

In terms of reconciling our calculations with previous experimental data<sup>8</sup>, one must be somewhat cautious. Clarke analyzed his results under the presumption that there would not be significant o-centering of the W ion within  $\text{WO}_6$  octahedra, which we believe to be incorrect: nevertheless, we believe that our tetragonal phase is consistent with collected data for his proposed cubic phase at high doping. Furthermore, our calculations deliberately neglect the effects of defects, chemical disorder, and other imperfections in the lattice.

Finally, we mention that the original motivation of our study was to investigate possible self-trapping behaviour of charge in this material. Excess electrons in the (low-temperature monoclinic) phase have been shown experimentally to self-trap, forming polarons<sup>26</sup>. We found no localisation of charge or deformation (polaron formation) in any of our calculations. This null result is of some interest, but should not be taken to mean that polarons do not form in this material; it is arguable that either the supercell used is too small to observe polaron localisation, or that the LDA will underestimate the binding energy of a polaron (thus causing it not to be a stable state of the system): further study is needed in this area.

## V. CONCLUSIONS

The main conclusion that we draw from our calculations is that the experimentally observed structural distortions induced in  $\text{Na}_x\text{WO}_3$  (type bronzes by increasing doping) are predominantly electronic in nature. By using our methodology of adding electrons to  $\text{WO}_3$  without also adding Na atoms, we have removed any possible structural/disorder effect caused by the  $\text{Na}^+$  cations on the A sites within the structure. Therefore, given that our calculations reproduce the experimentally observed sequence of symmetries upon doping ((i) Monoclinic (Pc and  $P2_1/c$ ); (ii) Orthorhombic (Pnma); (iii) Tetragonal ( $P4/nmm$ ); (iv) cubic aristotype ( $Pm3m$ )) we conclude that the effect of the  $\text{Na}^+$  cations on the structure must be small. Indeed, this is not unexpected. Following the classification of Robin and Day<sup>30</sup>, as mentioned by Bersuker<sup>31</sup>,  $\text{NaWO}_3$  is a good example of pure electronic doping; there is complete transfer of the donated Na electron over to the  $\text{WO}_3$  sublattice since the 3s band of Na lies well above the 5d-antibonding band from W.

Finally, we propose that these materials present interesting opportunities for future experimental and theoretical study, given the degree of structural control that can be gained from doping or substitution. In particular, the "quenching out" of polyhedral rotation (and hence the opening of channels within the structure) may have effects on diffusion and ion intercalation in these structures.

## A cknow ledgm ents

We would like to thank colleagues within the Mineral Physics group for technical assistance, and Dr. Martin Dove, Dr. William Lee, Dr. Simon Redfern, Prof. Ekhard Salje, and Prof. James Scott for fruitful discussions. Nicola Spaldin thanks the Earth Sciences Department

at Cambridge University for their hospitality during her recent sabbatical leave, and the U.S. National Science Foundation for financial support under grant number DMR-0312407. Andrew Walkingshaw wishes to acknowledge financial support from the Engineering and Physical Sciences Research Council, United Kingdom.

Permanent address: Materials Department, University of California, Santa Barbara, CA 93106

- <sup>1</sup> C. G. Granqvist, ed., *Handbook of Inorganic Electrochromic Materials* (Elsevier, Amsterdam, 1995).
- <sup>2</sup> A. S. Yu, N. Kumagai, Z. L. Liu, and J. Y. Lee, *J. Sol. Stat. Electrochem.* **2**, 394 (1998).
- <sup>3</sup> J. J. Berzelius, *J. Chem. Phys. (Berlin)* **16**, 476 (1816).
- <sup>4</sup> B. W. Brown and E. Banks, *J. Am. Chem. Soc.* **76**, 963 (1954).
- <sup>5</sup> P. M. S. Monk, R. J. Mortimer, and D. R. Rosseinsky, *Electrochromism: Fundamentals and Applications* (VCH Verlagsgesellschaft, Weinheim, 1995).
- <sup>6</sup> G. Kohlstrung, *Phys. Stat. Sol.* **2**, 85 (1962).
- <sup>7</sup> A. M. Glazer, *Acta Crystallogr., Sect. B* **28**, 3384 (1972).
- <sup>8</sup> R. Clarke, *Phys. Rev. Lett.* **39**, 1550 (1977).
- <sup>9</sup> F. Cora, M. G. Stachiotti, C. R. A. Catlow, and C. O. Rodriguez, *J. Phys. Chem. B* **101**, 3945 (1997).
- <sup>10</sup> M. G. Stachiotti, F. Cora, C. R. A. Catlow, and C. O. Rodriguez, *Phys. Rev. B* **55**, 7508 (1997).
- <sup>11</sup> N. A. Hill, *J. Phys. Chem. B* **104**, 6694 (2000).
- <sup>12</sup> A. H. Jelm, C. G. Granqvist, and J. M. Wills, *Phys. Rev. B* **54**, 2436 (1996).
- <sup>13</sup> G. A. de Wijk, P. K. de Boer, R. A. de Groot, and G. Kresse, *Phys. Rev. B* **59**, 2684 (1999).
- <sup>14</sup> F. Detraux, P. Ghosez, and X. Gonze, *Phys. Rev. B* **56**, 983 (1997).
- <sup>15</sup> P. Ordejon, E. Artacho, and J. M. Soler, *Phys. Rev. B* **53**, 10441 (1996).
- <sup>16</sup> J. M. Soler, E. Artacho, J. D. Gale, A. Garcia, J. Junquera, P. Ordejon, and D. Sanchez-Portal, *J. Phys. Condens. Matter* **14**, 2745 (2002).
- <sup>17</sup> P. Hohenberg and W. Kohn, *Phys. Rev. B* **136**, 864 (1964).
- <sup>18</sup> J. P. Perdew and A. Zunger, *Phys. Rev. B* **23**, 5048 (1981).
- <sup>19</sup> W. Kohn and L. J. Sham, *Phys. Rev. A* **140**, 1133 (1965).
- <sup>20</sup> N. Trouiller and J. L. Martins, *Phys. Rev. B* **43** (1993).
- <sup>21</sup> L. Kleinman and D. M. Bylander, *Phys. Rev. Lett.* **48**, 1425 (1982).
- <sup>22</sup> E. Anglada, J. M. Soler, J. Junquera, and E. Artacho, *Phys. Rev. B* **66**, 205101 (2002).
- <sup>23</sup> S. G. Louie, S. Froyen, and M. L. Cohen, *Phys. Rev. B* **26** (1982).
- <sup>24</sup> J. Moreno and J. M. Soler, *Phys. Rev. B* **45**, 13891 (1992).
- <sup>25</sup> H. Monkhorst and J. D. Pack, *Phys. Rev. B* **13**, 5188 (1976).
- <sup>26</sup> E. K. H. Salje, S. Rehmann, F. Pobell, D. Morris, K. S. Knight, T. Hemmendorf, and M. T. Dove, *J. Phys. Condens. Matter* **9**, 6564 (1997).
- <sup>27</sup> O. Loopstra and H. M. Rietveld, *Acta Crystallogr., Sect. B* **25** (1975).
- <sup>28</sup> E. K. H. Salje and K. Viswanathan, *Acta Crystallogr., Sect. A* **31** (1975).
- <sup>29</sup> S. Tanisaki, *J. Phys. Soc. Jpn* **14**, 566 (1960).
- <sup>30</sup> M. B. Robin and P. Day, *Adv. Inorg. Chem. Radiochem.* **10**, 247 (1967).
- <sup>31</sup> I. B. Bersuker, *Electronic Structure and Properties of Transition Metal Compounds: Introduction to the Theory* (Wiley and Sons, New York, 1996).